An Experimental Study of the Small-Scale Variability of Rainfall

ALI TOKAY

Joint Center for Earth Systems Technology, University of Maryland, Baltimore County, Baltimore, and NASA Goddard Space Flight Center, Greenbelt, Maryland

KURTULUŞ ÖZTÜRK

Turkish State Meteorological Service, Ankara, Turkey

(Manuscript received 2 February 2011, in final form 11 July 2011)

ABSTRACT

Small-scale variability of rainfall has been studied employing six dual rain gauge sites at Wallops Island, Virginia. The rain gauge sites were separated between 0.4 and 5 km, matching the beamwidth of Tropical Rainfall Measuring Mission (TRMM) and Global Precipitation Measurement (GPM) precipitation radars. During a 2-yr observational period, over 7100 rainy samples were received at 5-min integration. A single gauge did not report as high as 67% of the time when at least one of the other gauges had rainfall in one of the seasons. Since rainfall from one of the six rain gauges is sufficient for the rainy footprint from a satellite, this demonstrates the common occurrence of the partial beamfilling. For the periods where all gauges were reporting rainfall, a single gauge had at most 13% difference from the areal average rainfall in one of the seasons. This suggests that at the spatial scale of 5 km, the variability caused by the rain gradient is relatively less important than the variability arising from a partially filled footprint. During the passage of frontal systems and tropical cyclones, the beam was filled by rain most of the time and this resulted in relatively higher correlation distances. The correlation distance had a sharp drop off from 45 km in moderately variable rainfall to 3 km in highly variable rainfall and ranged from 5 to 35 km between the different seasons. This demonstrates its highly variable nature. Considering temporal sampling, the monthly rainfall error was 35% and 73% for 3-hourly and twice-daily observations, respectively.

1. Introduction

Satellite measurements are the only option to estimate surface precipitation over oceans and the vast majority of land surfaces that lack precipitation-measuring instruments. The precipitation retrieval algorithms from active and passive microwave sensors on board polar orbiting earth observing satellites rely on a number of assumptions regarding precipitation microphysics and suffer from the nonuniform characteristics of precipitation within their respective footprints.

The Tropical Rainfall Measuring Mission (TRMM), a joint project between the National Aeronautics and Space Administration (NASA) and the Japanese Aerospace Exploration Agency (JAXA), is dedicated to precipitation measurement over the tropics and subtropics. The TRMM satellite carries the first precipitation radar (PR) and nine-channel microwave sensors, among other instruments (Kummerow et al. 1998). The PR provides the vertical profile of reflectivity, which is corrected for attenuation (Iguchi et al. 2000). Nonuniform beamfilling is a key source of error for this attenuation correction since the reflectivity profile for the inhomogeneous rain differs from that of homogeneous rainfall, even when the footprint average rainfall is the same (Takahashi et al. 2006). To conserve fuel and thus extend its lifetime, the orbital altitude of the TRMM satellite was boosted from 350 to 402.5 km in August 2001. The PR near-nadir field of view then increased from 4.3 to 5.0 km, making nonuniform beamfilling a more serious problem for the PR algorithm (Liao and Meneghini 2009).

The precipitation retrieval algorithms from the TRMM microwave imager (TMI) and many other passive microwave sensors employ a radiative transfer and cloud model or PR data and use explicit physical assumptions to derive relations between brightness temperature and

Corresponding author address: Ali Tokay, NASA Goddard Space Flight Center, Code 613.1, Greenbelt, MD 20771.
E-mail: ali.tokay-1@nasa.gov

DOI: 10.1175/JHM-D-11-014.1

© 2012 American Meteorological Society

rainfall. Varma et al. (2004) showed a significant disagreement between the observed brightness temperature and rainfall at two different frequencies of the TMI in convective rain. They attributed this disagreement to the differences in the instantaneous field of view. Prior to this study, Kummerow (1998) recognized that the homogeneous rainfall assumption is the largest uncertainty in physically based precipitation retrieval algorithms. The instantaneous field of view of the TMI is elliptical and at the earth's surface, prior to boost, had a diameter in the cross-track direction of 4.1 km and a down-track diameter of 6.7 km at 85.5 GHz at vertical polarization (Kummerow et al. 1998). The TMI instantaneous field of view is larger at lower frequencies, reaching 60.1 and 36.4 km in down-track and cross-track directions, respectively, at 10.65 GHz at horizontal polarization. Like the PR, the increase in the instantaneous field of views after the boost exacerbates the beamfilling problem particularly for physically based precipitation retrieval algorithms.

TRMM is one of the oldest active satellites in space within NASA's Earth Science Observing System. The next satellite that is dedicated to precipitation measurements, Global Precipitation Measurement (GPM), is scheduled to launch its core satellite in 2013. The GPM core satellite will carry a dual-frequency precipitation radar (DPR) and a 13-channel microwave imager (GMI). The core satellite will fly at a 405-km altitude and the DPR will have a 5-km footprint at nadir (Nakamura and Iguchi 2007). The instantaneous field of view of the GMI will range from 4.4×7.3 km^2 at 183.3 GHz to 19.4×32.2 km^2 at 10.65 GHz (Hou et al. 2008). Both TRMM and GPM satellites are in a non-sun-synchronous orbit, which allows them to cover the globe spatially within their altitude of inclinations. Temporal sampling is limited to twice-daily sampling on the earth's surface. To enhance temporal sampling, the precipitation estimates from various microwave sensors have been combined into a single product. The TRMM Multisatellite Precipitation Analysis (TMPA) is a 3-hourly $0.25° \times 0.25°$ precipitation product that covers $\pm 50°$ latitude (Huffman et al. 2007). The TMPA merges the microwave sensor precipitation estimate with a microwave-calibrated infrared precipitation estimate. It also includes gauge rainfall at a monthly scale. With the additional satellites that carry microwave imagers, GPM is committed to providing a precipitation estimate every 1–2 h at every location on land and every 2–4 h over ocean (Hou et al. 2008).

Ground validation is one of the main components of the TRMM and GPM projects. The direct comparison between ground-based and spaceborne precipitation estimates helps to evaluate the performance of the satellite algorithm (Liao et al. 2001; Wolff et al. 2005; Liao and Meneghini 2009). Various assumptions of the satellite algorithm can be further evaluated by employing ground-based observations from field campaigns. Kummerow (1998), for instance, employed shipborne radar observations from the Tropical Ocean Global Atmosphere Coupled Ocean Atmosphere Experiment (TOGA COARE) to examine the nonuniform beamfilling effect on microwave precipitation retrievals. The same radar dataset has been used to examine the factional rain area and distribution of rainfall within the TMI field of view (Varma et al. 2004).

Rain gauges are an integral component of the satellite precipitation algorithm validation studies. They play an important role in constructing and validating radar rainfall estimates (Wolff et al. 2005). Dense rain gauge networks that are operated in field campaigns help to determine the variability of rainfall within the scale of a radar pixel and satellite footprint. The TRMM postlaunch field campaigns in east-central Florida and the southwest Amazon basin of Brazil included such dense rain gauge networks. Gebremichael and Krajewski (2004) used both gauge networks to evaluate the ability of the radar-derived products to characterize the small-scale (less than 20 km) variability of rainfall. Habib and Krajewski (2002) and Datta et al. (2003) also used the gauge network in east-central Florida for studying the variability of rainfall within the scale of a radar pixel. The former study was interested in the rainfall variability at time scales of 1 h or less, while the later study examined the variability for an event as well as for 5- and 30-day periods. These dense rain gauge networks included collocated gauges, which helped to determine the gauge random error. At the same time, the experiments were relatively short (approximately 2 months) to determine the variability for different types of storms and for seasons and longer climatological periods. Rain gauge networks that have been operating 2 yr or longer allow for studying the small-scale variability between the different years. However, operations are costly and the gauge maintenance can be challenging, especially in remote locations.

The TRMM satellite validation office has been operating a gauge network at NASA Kennedy Space Flight Center (KSC) for over a decade. Wang and Wolff (2010) employed 1 yr of these gauge observations to evaluate the TRMM radar rainfall product. The distances between the rain gauges at KSC range from approximately 2 to 32 km distance with no collocated gauges at any site. Among other rain gauge networks that are relevant to studying the rainfall variability within the satellite field of view and radar pixel are the University of Oklahoma Environmental Verification and Analysis Center (EVAC)

PicoNet, which included 24 dual- and 1 five-collocated gauges. Ciach and Krajewski (2006, hereafter CK06) used two years of this dataset to model the spatial correlation of rainfall over a nearly square area where the intergauge separation distances ranged from just under 0.5 to about 3.4 km. The site previously hosted 15 collocated gauges to study the local random errors of tipping-bucket gauges (Ciach 2003). Villarini et al. (2008, hereafter VMKM08) and Villarini and Krajewski (2008), on the other hand, used a unique gauge dataset from southwest England to study the spatial and temporal sampling uncertainties of rainfall. The 6-yr dataset included 50 rain gauges where the separation distance ranged from 0.5 to 15 km. The rain gauges were deployed during the Hydrological Radar Experiment (HYREX; Moore et al. 2000). It should be noted that all the gauges mentioned above were tipping bucket and the studies did not include mixed phase or frozen precipitation.

This study uses a rain gauge network at NASA's Wallops Flight Facility (WFF), Wallops Island, Virginia (37.84°N, 75.48°W). The main objective of this study is to investigate the spatial variability of rainfall within a 5-km distance, which coincides with approximate diameter of the instantaneous field of view (IFOV) of the TRMM PR. The GPM DPR will have similar IFOVs at both Ku- and Ka-band frequencies. A description of the dataset and instrumentation can be found in section 2. The nonuniform beamfilling is discussed in section 3, while section 4 presents the errors in monthly rainfall due to temporal sampling of satellite measurements. A spatial correlation function and the variability of its parameter for different subsets of observations are discussed in section 5. The dependence of the spatial correlation function on various integration periods is also given in this section. Conclusive remarks will be presented at the end.

2. Rainfall measurements

As part of the TRMM satellite validation program, a dense rain gauge network has been operated at NASA WFF for 2 yr starting from December 2005. The network consisted of six dual Met One Inc. tipping-bucket sites (Fig. 1). The gauges were aligned nearly in a straight line across Wallops Island where the minimum and maximum distances were 0.4 and 5.0 km, respectively (Fig. 2). The Met One gauge has 20.3-cm diameter orifice, and each tip corresponds to 0.254-mm rainfall. The time stamp of the tip was recorded to a battery-operated MadgeTech datalogger. The logger was located inside a waterproof box that fit inside the gauge cylinder. A technician visited each gauge every month—essential to maintain a high-quality dataset. The failure of one of the two collocated gauges was rarely observed during the 2-yr-long experiment period. A continuous gauge record of rainfall was available at each site, and the G03 site had a continuous record for both collocated gauges throughout the experiment.

FIG. 1. A picture of the dual rain gauge site at NASA Wallops Flight Facility, Wallops Island, Virginia.

During the experiment period, gauges recorded 1960 mm of rainfall in more than 7100 rainy samples when the rainfall was averaged between the six gauge sites. The rainy samples were based on 5-min accumulation periods at 0.5-mm (two tips) threshold. Although longer accumulation periods and other rain–no-rain thresholds were also included as a sensitivity study, 5-min integration with 0.5-mm threshold was considered as the base of this study. Since the rain gauges were not heated, the rare snow events were excluded. False tips typically occur following a snow event once the snow in the gauge melts and multiple tips in a minute are observed when no precipitation is reported by nearby operational gauges. These false tips were carefully eliminated from the record. While 2-yr accumulation matched with the local climatology, there were noticeable differences between the observed and the climatological rainfall on monthly, seasonal, and yearly totals (Figs. 3a–c). Only 45% of the mean seasonal rainfall fell in spring 2006 in drought conditions, while Hurricane Ernesto (2006) contributed abundant rainfall during autumn 2006 where rainfall was 2.3 times the seasonal average. This demonstrates that 2-month-long field campaigns may not be adequate to collect the sufficient amount of rainfall at a midlatitude site unless the rainfall climatology indicates abundant rainfall in a given season. Wallops Island receives precipitation from frontal systems, air mass convection, and remnants of tropical cyclones and is one of the rainiest locations based on annual precipitation in the continental United States outside the southeastern states and the Pacific Northwest.

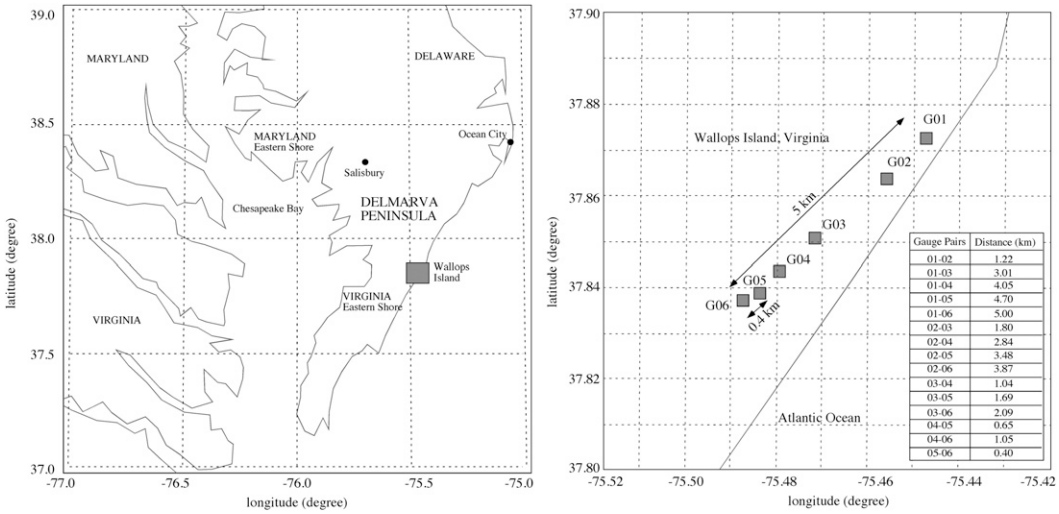

FIG. 2. NASA Wallops Flight Facility rain gauge network. (left) The greater area of the mid-Atlantic and (right) the expanded Wallops Island site. The distance between the paired gauge sites is also presented in a table form.

3. Nonuniform beamfilling

The nonuniform beamfilling consists of the variability and partial coverage of rainfall within the beam. Although these two factors occur simultaneously, we tried to determine these effects separately. The percent occurrence, which is the ratio of rain occurrence of a single gauge to beam rainfall, is considered to be the measure for partial coverage. Beam rainfall is the average rainfall between the six gauge sites for 5-min totals. Here, the beam rainfall is calculated even if only one gauge reported rainfall. The 5-min rain total is considered to be shortest reliable gauge rainfall (Habib and Krajewski 2002) and one gauge from each site is selected for this segment of the study. The dataset is partitioned for 15 different climatological periods including eight seasons, four 6-month periods, two years, and one 2-yr period.

The gauge at the lower end of the network (G06) had the highest percentage of rain occurrence for all seasons except for two summers where the gauge at the upper end of the gauge network (G01) had the highest occurrences (Fig. 4). The difference of rain occurrence between G06 and other gauges was larger than 1% in all seasons except summers, becoming nearly 10% during spring 2007. It was interesting that G06 received distinctly higher rain occurrences than its neighboring gauge (G05), which was only 0.4 km away. For all seasons, at least one of the gauges had less than 50% rain occurrence and none of the gauges had rain occurrence more than 67%. Moreover, all the gauges were below 50% rain occurrence during spring 2006. This demonstrates the significance of partial coverage within a 5-km footprint.

The intrabeam variability of rainfall is determined by taking the ratio of the difference between the individual gauge and complete beam rainfall to the complete beam rainfall. The complete beam rainfall is the average rainfall of six gauges when all the gauges report rainfall for the 5-min accumulation period. The complete beam rainfall differs from beam rainfall, which requires just one of the six rain gauges reporting rainfall. G06 had the highest positive deviation from complete beam average for all seasons except autumn 2006 (Fig. 5). The G06 had also the maximum deviation (13%) from complete beam average in autumn 2007. G01, on the other hand, had the maximum negative deviation (13%) from complete beam average in summer 2007, but the neighboring gauges (G02 and G03) had the highest negative deviations for other seasons. This segment of the study reveals that at the spatial scale of 5 km, partial beamfilling from intrabeam variability is relatively less important than that from rain occurrence.

4. Temporal sampling

Polar-orbiting-satellite-based climate rainfall products suffer from temporal sampling errors. The TRMM climate products, which include PR (3A25), TMI (3A11 and 3A12), and combined PR–TMI (3B31) monthly precipitation, are based on twice-daily overpasses and are constructed either at 5° × 5° or 0.25° × 0.25° resolution. To reduce the temporal sampling errors and increase the accuracy of climate rainfall products, efforts have been made through combining multisatellite precipitation products. The TMPA, another TRMM standard climate product, is based on a 3-hourly multisensor precipitation analysis as noted in the introduction. It is

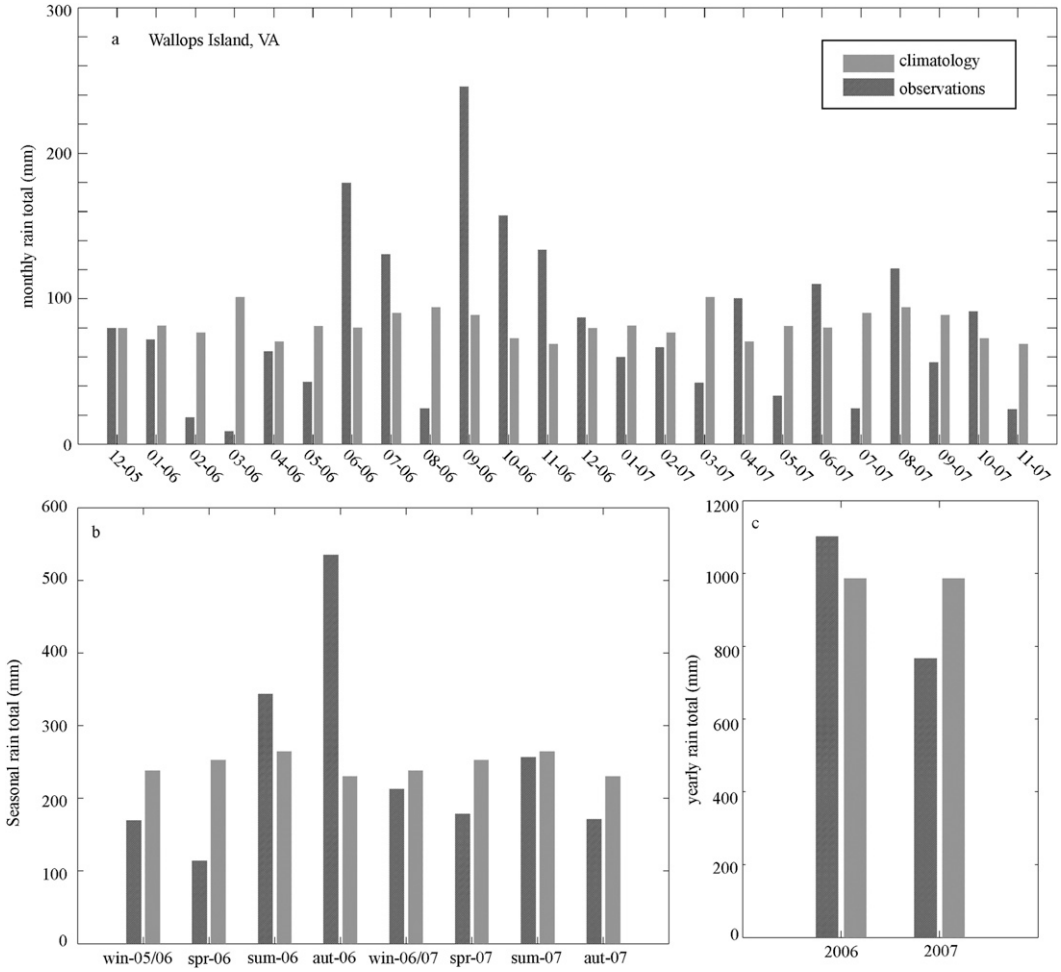

FIG. 3. Areal average rainfall accumulation (dark bars) and precipitation climatology (light bars) for NASA Wallops Flight Facility for a (a) month, (b) season, and (c) year.

anticipated that the GPM standard climate products will be similar to TRMM, and monthly precipitation will primarily rely on the use of multisatellite-based precipitation estimates.

The temporal sampling errors of monthly precipitation totals are investigated by employing the gauge network introduced above. The true monthly rainfall (rain_t) is based on the average rainfall from six gauge sites for 5-min accumulations. One gauge from each gauge site is used to determine rain_t. The monthly rainfall is recalculated for different temporal samplings ranging from 10 min to 12 h. These estimated monthly rain amounts (rain_e) assume that the rainfall was uniform for the period between the consecutive observations. The percent absolute error is then calculated for a given month:

$$\text{percent_absolute_error} = \frac{|\text{rain}_t - \text{rain}_e|}{\text{rain}_t} \times 100. \qquad (1)$$

The median, mean, and standard deviation of the percent absolute errors are calculated employing 24 monthly accumulations (Fig. 6). For a polar-orbiting satellite that samples every place within its orbit twice a day, the percent absolute error is 73% on average. If the monthly precipitation is based on 3-hourly observations, the percent absolute error is about 35% on average. As mentioned in the introduction, it is expected that GPM will provide a precipitation estimate every 1–2 h on land and every 2–4 h over ocean. The percent absolute error is 19% on average for hourly sampling, while 26% and 40% errors are expected for 2- and 4-h samplings on average.

It should be noted that the percent absolute errors presented above do not directly address the temporal sampling errors in TRMM and GPM standard climate products. The dataset used in this study does not include mixed precipitation and/or snow, and the gauge-based areal average rainfall could be well below the satellite's minimum detectable precipitation, which is about

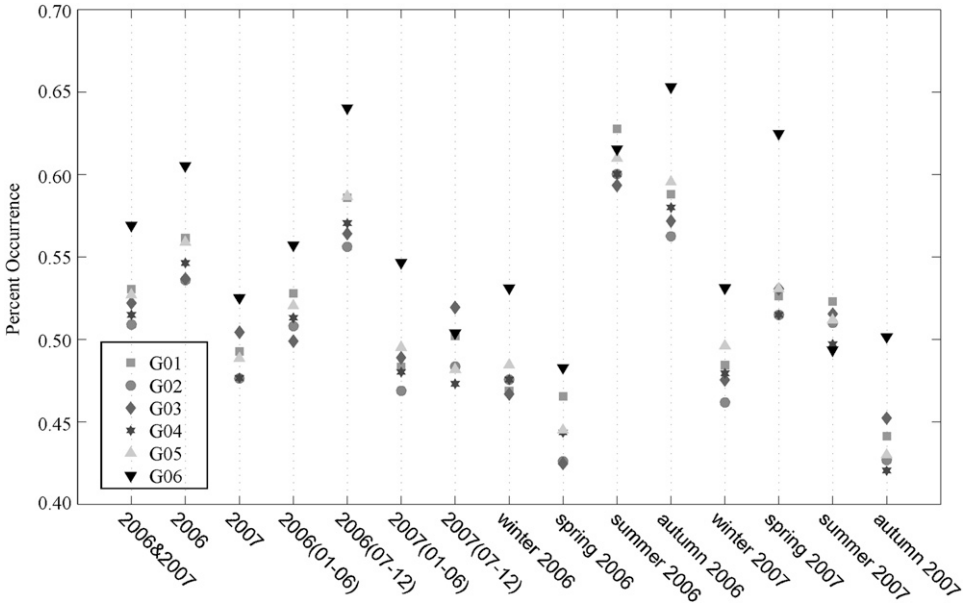

FIG. 4. Percent occurrence of gauge rainfall with respect to the beam rainfall, which is the areal average rainfall between the six gauge sites for 5-min accumulation. Percent occurrence is given for eight seasons, four 6-month periods, two years, and a 2-yr period.

0.5 mm h^{-1} for TRMM PR and is expected to be 0.2 mm h^{-1} for GPM DPR (R. Meneghini, 2011, personal communication). More importantly, the TRMM and GPM standard climate products are generated on a much larger spatial scale than the 5 km^2.

5. Spatial variability

The Pearson correlation coefficient (r) is computed for the gauge pairs between the six different sites where one gauge from each gauge site is used. The correlations are computed for 15 different climatological subsets, but the dataset is also grouped for two meteorological regimes and for three different uniformity of rainfall categories, totaling 20 subsets. A three-parameter stretched exponential model is selected to determine the intergauge correlations and is expressed as

$$r = r_0 \exp\left[-\left(\frac{d}{d_0}\right)^s\right], \tag{2}$$

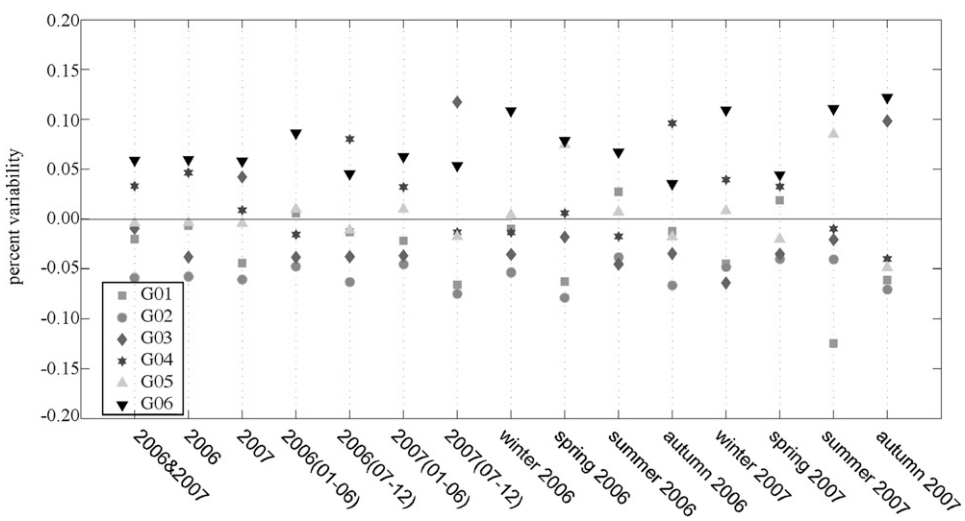

FIG. 5. As in Fig. 4, but for percent variability.

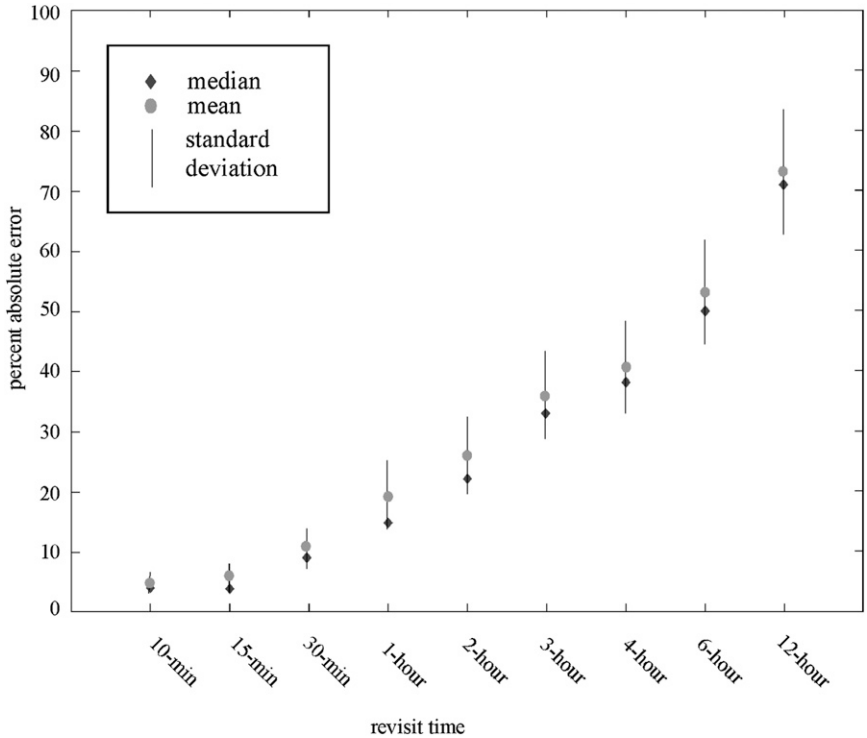

FIG. 6. Percent absolute error of monthly rainfall for a remote sensing precipitation measurements that sample the experiment area ranging from 10-min to 12-h intervals.

where r_0 is the nugget parameter, d is the distance between the two gauge sites, d_0 is the correlation distance, and s is the shape parameter. This parametric model has been used in the past (Habib et al. 2001; Habib and Krajewski 2002; Gebremichael and Krajewski 2004; Krajewski et al. 2003; VMKM08) and its parameters are quite sensitive to each other. If the shape and nugget parameters are one, then Eq. (2) is the simple exponential model where d_0 is the e-folding distance (CK06). Even when shape parameter is not one, d_0 is still the e-folding distance when d is equal to d_0. In the absence of collocated gauges, Wang and Wolff (2010) estimated r_0 and d_0 by setting the shape parameter to 1.0. As an alternative, it is feasible to estimate all three parameters, but the model fitting is not successful with high values of minimum root-mean-square error (rmse) (CK06). The minimum rmse is ultimately the measure of the goodness of fit, which determines the values of estimated parameters. In this study, nonlinear least squares are employed for fitting of the stretched exponential function.

The nugget parameter is the correlation coefficient between the rain rates of the collocated gauges and is related to the discrepancies between the gauge readings as being local random errors, which depend highly on the rain intensity and period of data integration (Ciach 2003). In this study, the nugget parameter was determined based on data from the G03 site where both gauges operated with no failure during the experiment. The nugget parameter increased with the integration period from 0.97 at 5-min accumulation to 0.99 at 20-min accumulation and remained around 0.99 for longer accumulation periods (Fig. 7a). VMKM08 found the nugget parameter of 0.96 for 5-min accumulation with an asymptotical increase for longer integration periods. The increase of nugget parameter with integration period was also evident in the CK06 study, but the correlations were above 0.99 for 5-min and longer accumulations.

The correlation distances also show an increasing trend with integration time (Fig. 7b). The distances remain less than 80 km up to 30-min integration, and range between 170 and 230 km for longer integration periods (except at 12 h where it is nearly 320 km). These very large correlation distances should be interpreted with caution. Considering two gauge stations that are separated by 170 km, one cannot expect a nearly 0.37 correlation in hourly rainfall even though this is what the results suggest if the nugget parameter is taken as 1.0. VMKM08 also showed relatively gradual increase of correlation distance with integration periods up to 30 min, while the increase was noticeably faster for longer integration periods. However, the correlation distances were much shorter, reaching 110 km at 12 h. CK06, on the other hand, showed a similar

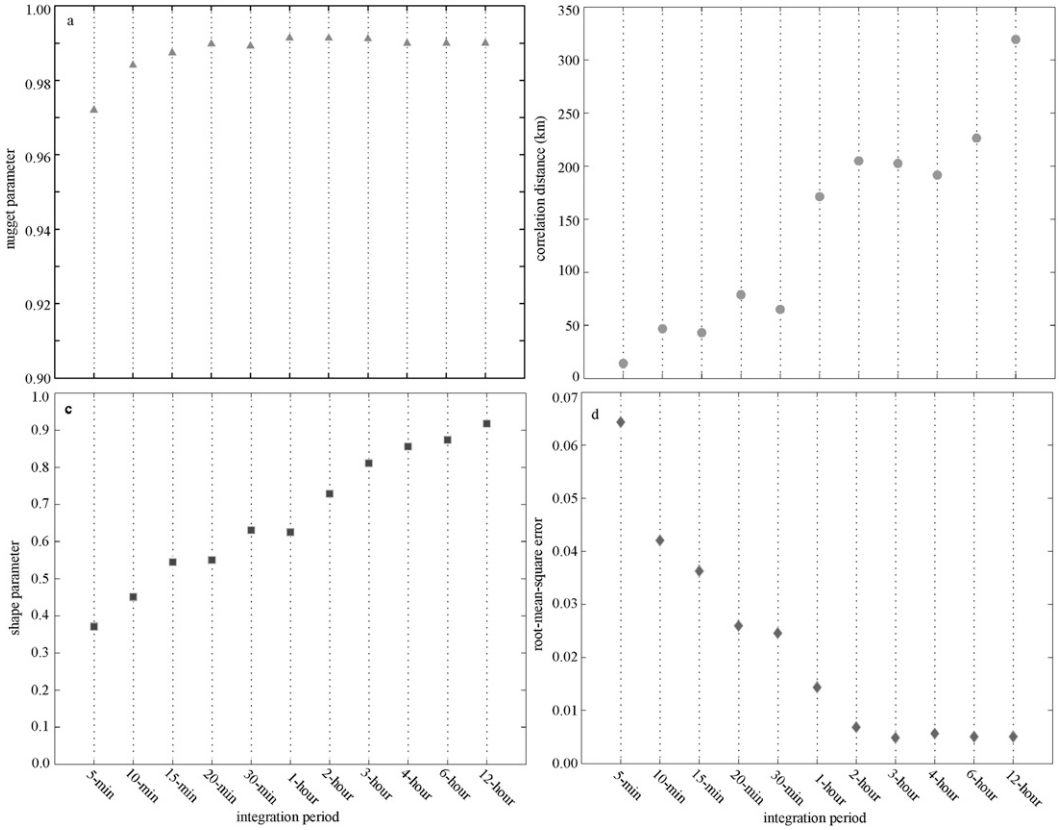

FIG. 7. Dependence of (a) nugget parameter, (b) correlation distance, (c) shape parameter of the exponential function, and (d) rmse on the averaging time scale ranging from 5 min to 12 h.

trend with shorter correlation distances than the VMKM08 study. The increase of the correlation distances with the integration time is consistent with the predictions from certain theoretical models of precipitation statistics (Bell and Kundu 1996; Kundu and Bell 2003).

The shape parameter increases with the integration from 0.37 at 5 min to 0.92 at 12 h (Fig. 7c). A similar range, but first rapid and then gradual increase with a break point of 30-min period, was reported in VMKM08. CK06, on the other hand, displayed a trend similar to the shape parameter increase of VMKM08, but the range was between 1.1 and 1.6. The rmse decreases sharply from 5-min (0.064) to 2-h integration periods (0.007) and remains less than 0.006 for longer integration periods (Fig. 7d). CK06 showed a similar decrease of rmse with integration periods as well.

The scatter of correlations of the paired gauge rainfall around the exponential fit is a visual inspection of the goodness of fit (Fig. 8). The scatter is noticeably reduced from 5- to 15-min integration, and is very tight around the exponential fit at 3-h integration. At a distance of 5 km, the correlation of the functional fit is just below 0.5 at 5-min integration, while it is 0.95 at 3-h integration. The VMKM08 study resulted in 0.53 and 0.88 correlations at 5-min and 3-h integrations, respectively, at a distance of 5 km. The CK06 study, on the other hand, suggested 0.59 and 0.90 correlations at 5-min and 3-h integrations, respectively, at a distance of 5 km. As noted in the introduction, the maximum gauge spacing was less than 5 km in CK06, while the VMKM08 gauge network extends up to 15 km.

VMKM08 compared their findings with CK06 and pointed out the differences in experimental design, which included the number of gauges and their distances with respect to each other; precipitation type; sample size, which is related to the frequency of rain occurrence; and the duration of the experiment. These factors play a crucial role in the correlations between paired gauge rainfall and parameters of the stretched exponential model and, therefore, differences were expected between these experimental studies. In this study, the data quality is good since each site had dual gauges. The dual gauge platforms have advantages for years-long uninterrupted gauge record at a site (Krajewski and Smith 2002). As noted earlier, the experiment site received abundant rainfall from different synoptic systems. The

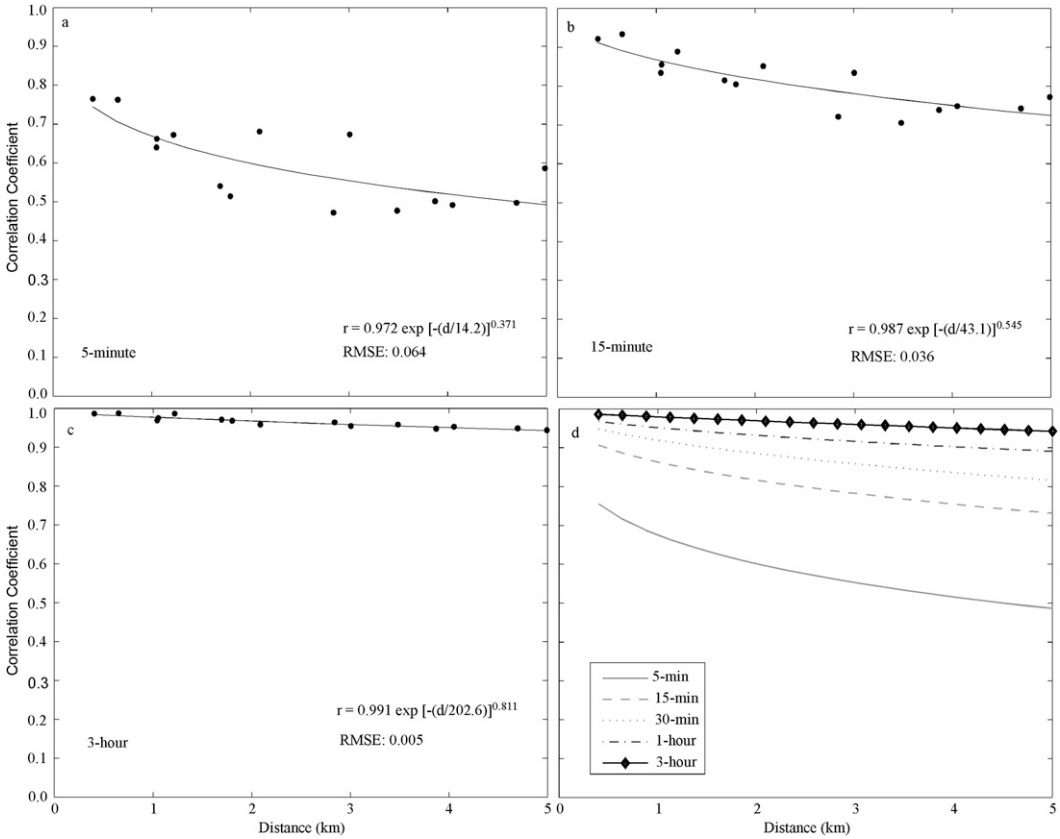

FIG. 8. Intergauge correlations (dots) and the fitted exponential function (curve) for (a) 5-min, (b) 15-min, and c) 3-h time averaging. The parameters of the exponential function and rmse are also given. (d) The exponential fits for the five different time averages indicated.

2-yr-long observations provided an adequate dataset to determine the fitting parameters under different synoptic configurations as well as for a season, 6-month period, and 1 yr. The dataset for each of the 20 subsets had at least 545 5-min samples.

The choice of rain–no-rain threshold is another factor that affects the parameters of the stretched exponential model. At 5-min integration, the correlation of functional fit ranges from 0.68 for a single tip (0.254 mm) rain–no-rain threshold to 0.17 for eight tips 2 mm) threshold at a distance of 5 km (Fig. 9). Since a single tip may occur at times where the bucket was mostly filled but tipped from a previous rain event or perhaps from strong winds, we considered two tips the most reliable database for this study. The higher rain–no-rain thresholds, on the other hand, ignored the rainfall from one of the paired gauges and therefore reduced the correlation.

There was a significant variability on the functional fit between the eight seasons (Figs. 10a,b). The most drastic variability occurred between the two autumn seasons. The correlations of functional fits were 0.92 for the shortest gauge separation distance for both autumn seasons, while the correlation of functional fits were 0.71 and 0.41 at the largest separation distance for autumn 2006 and autumn 2007, respectively (Fig. 10b). There was a significant variability between the two winter seasons as well (Fig. 10a). While the slopes of functional fits were about the same, the difference in correlations of the functional fits was greater than 0.1 between the shortest and the longest separation distances. The slopes of function fits were also the same but the correlations were noticeably different between the two summer seasons (Fig. 10b). The slopes of functional fits were quite different, crossing each other at 3.8-km distance between the two spring seasons (Fig. 10a).

The significant variability of functional fits was also evident between the two first 6 months of 2006 and 2007 (Fig. 10c). The correlations of functional fits were 0.88 and 0.89 for the shortest separation distance and 0.39 and 0.67 at the longest separation distance for the first 6-month periods of 2006 and of 2007, respectively. The correlations of function fits were within these bounds during the second 6-month periods of the same years (Fig. 10c). The slopes of functional fits were different

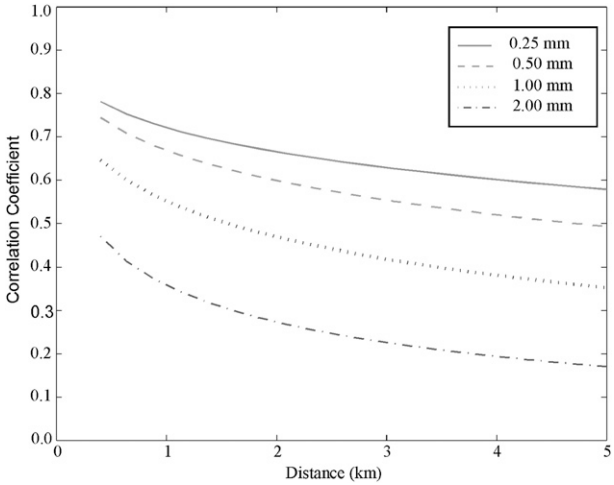

FIG. 9. Correlation of exponential fit for four different rain–no-rain thresholds.

between the second 6-month periods crossing each other at 2.5-km distance. The correlations were significantly different between the two years as well (Fig. 10d). The correlations were relatively lower during 2006 where the functional fit ranged from 0.70 at the shortest separation distance to 0.42 at the longest separation distance.

The correlations were noticeably higher in weather-event-based merged subsets than those for the entire dataset (Fig. 11a). The weather events were determined by examining surface weather maps. The passage of cold fronts from the west is frequently observed in the mid-Atlantic region. The region is also subject to the passage of remnants of tropical cyclones like Hurricane Ernesto (2006). At 5-km distance, the correlation of the functional fit was 0.76 and 0.72 in frontal events and tropical cyclones, respectively, as opposed to 0.50 in the entire dataset.

The correlations and their functional fit were substantially different for uniform, moderately variable, and highly variable observations (Fig. 11b). The uniformity of rainfall is determined based on the thresholds of the coefficient of variation (CV), which is the ratio of standard deviation to the areal mean rainfall. The categories of uniformity of rainfall are determined following Habib et al. (2009) and are uniform rain ($CV \leq 0.2$), moderately variable rain ($0.2 < CV \leq 0.5$), and highly variable rain ($CV > 0.5$). The functional fit in uniform

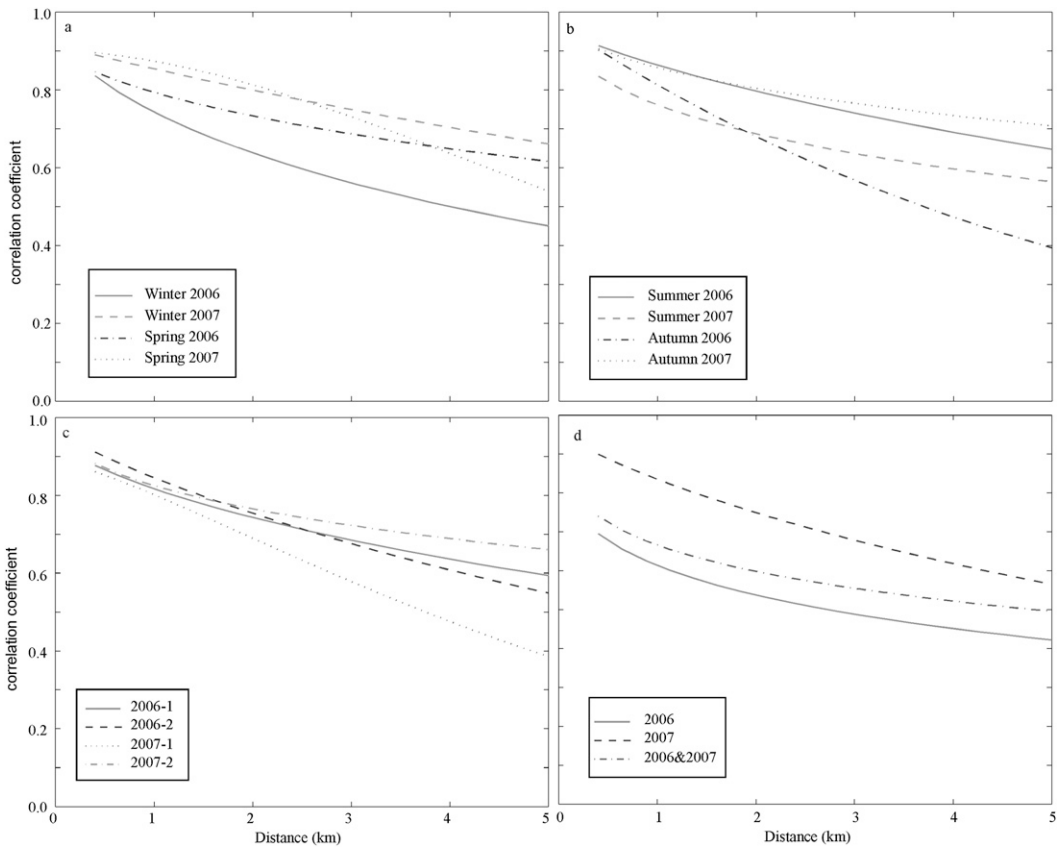

FIG. 10. Correlation of function fit for (a) winter and spring seasons, (b) summer and autumn seasons, (c) 6-month periods, and (d) year and 2-yr periods.

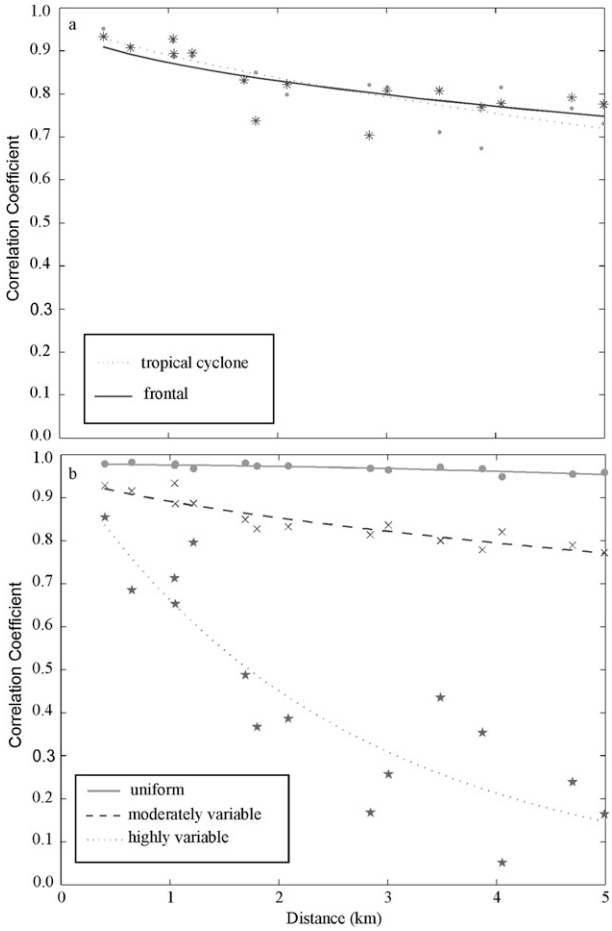

FIG. 11. Correlation of functional fit (a) tropical cyclone (solid) and frontal (dashed) cases, and (b) uniform, moderately variable, and highly variable cases. The correlation between paired gauges was also shown for (top) tropical cyclones (•) and frontal (∗) cases and for (bottom) uniform (•), moderately variable (×), and highly variable (★) cases.

rain resembles 3-h averaged function fit (Fig. 8c), as the correlations remained higher than 0.95 at any gauge separation distance. The correlations of functional fit of the moderately variable rainfall ranged between 0.93 at the shortest separation distance and 0.78 at the longest separation distance. The correlations of the functional fits of highly variable rainfall, on the other hand, had a wide range between the shortest and the longest separation distances as being 0.87 and 0.17 at these distances, respectively.

There have been a few studies where the gauges' observations were grouped based on uniformity, but as far as we know there was no study where the observations were grouped based on weather events. Habib and Krajewski (2002) grouped a dense network of rain gauge measurements in central Florida to light and heavy rain based on a coincident radar rainfall estimate. If the radar rainfall was less than 10 mm h^{-1}, it was considered light rain. Otherwise, it was called heavy rain. They reported the correlation distances of 4.6 and 2.5 km for a 15-min integration period for light and heavy rain, respectively. CK06 implemented a similar study for two different thresholds. While the correlations were higher for lighter rain at the 10 mm h^{-1} threshold, the reverse was true at the 3 mm h^{-1} threshold. The latter authors pointed out that the correlation functions are highly ambiguous when the observations were subsampled based on rain rate thresholds. The additional statistical dependences that were imposed on the subsampled data caused the ambiguity. CK06 also showed the storm-by-storm variability of correlation distance and shape parameter and examined the uniformity of rainfall by employing the correlations of the individual rain events at a 1-km distance for a 3-min integration period. The correlation of 0.9 was the breakpoint between low and high spatial variability. They reported correlation distances of 9.8 and 4.4 km for low and high spatial variability cases, respectively.

The parameters of the stretched exponential model showed noticeable differences between seasons, 6-month periods, and years as well as between different weather systems and different uniformity of rainfall. Among the seasons, the nugget parameter had its lowest value, 0.90, during the spring of 2007 and its second and third lowest values, 0.91 and 0.92, occurred during winter 2007 and spring 2006, respectively (Fig. 12a). The nugget parameter was quite low, 0.88, during the first 6 months of 2007 and was also 0.92 during 2006. It was 0.95 or above for the other study periods.

The correlation distance ranged from 6 km in the autumn of 2006 to 35 km in the autumn of 2007 between the seasons when it is determined for the best goodness of fit (Fig. 12b). For the 6-month periods, the correlation distance ranged from 6 km in the first 6-month period of 2007 to 29 km in the second 6-month of 2007 and it was within the range of these distances for the yearly and 2-yr periods. Interestingly, the correlation distance was quite high, 53 km, for frontal systems, while it was 24 km for tropical cyclones. Moderately variable rainfall resulted in the correlation distance of 45 km—nearly 4 km higher than correlation distance of the uniform rainfall. One may expect that the correlation distance is higher for uniform rain than moderately variable rain. The differences in nugget parameter and rmse may account for the rather low value of the correlation distance in uniform rain. The highly variable rainfall had only 3-km correlation distance.

As noted earlier, the parameters of the exponential fit are related to each other. In the absence of collocated gauges, a predetermined nugget or shape parameters

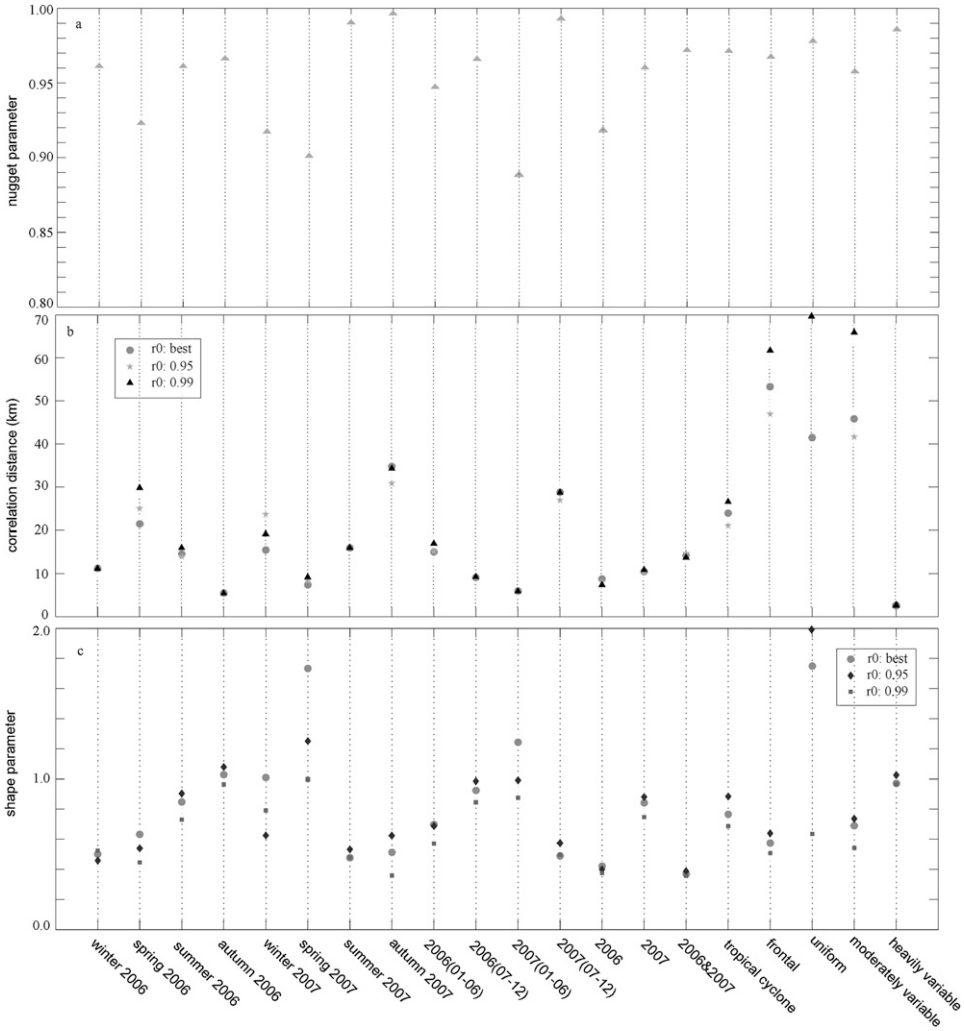

FIG. 12. Parameters of exponential fit and rmse for eight seasons, four 6-month periods, two years, and a 2-yr period as well as for frontal, tropical cyclone, uniform, moderately variable, and highly variable cases. (a) Nugget parameter, (b) correlation distance for the best and selected nugget parameters, (c) shape parameter, (d) correlation distance for the best and selected shape parameters, (e) rmse for the best and selected nugget parameters, and (f) as in (e) but for selected shape parameters.

may be assumed to determine the correlation distance in Eq. (2). Wang and Wolff (2010) study, for instance, found a very low nugget parameter, 0.72, for the predetermined shape parameter of 1 for a 5-min accumulation. In this study, two predetermined nugget (0.95 and 0.99) and shape (0.75 and 1.00) parameters were selected to test the sensitivity of correlation distance to preconditioned cases.

The correlation distance showed noticeable differences between its best and predetermined nugget parameter-based values in most of the observational periods (Fig. 12b). It increased 14% and 28% from its best value when the nugget parameters were fixed at 0.95 and 0.99, respectively, during spring 2006. For the frontal systems, the correlation distance decreased and increased 13% from its best value when the nugget parameters were 0.95 and 0.99, respectively. The correlation distance became unrealistically high for uniform precipitation for the fixed nugget parameters and was almost insensitive to the fixed nugget parameters for several seasons, 6-month, and longer climatological periods as well as for highly variable rain.

The difference between the collocated-gauge-based and predetermined nugget parameters was not necessarily correlated to the difference in correlation distances. This is probably due to the fact the shape parameter also changes and the rmse differs. The shape parameter shows substantial differences between its best and predetermined

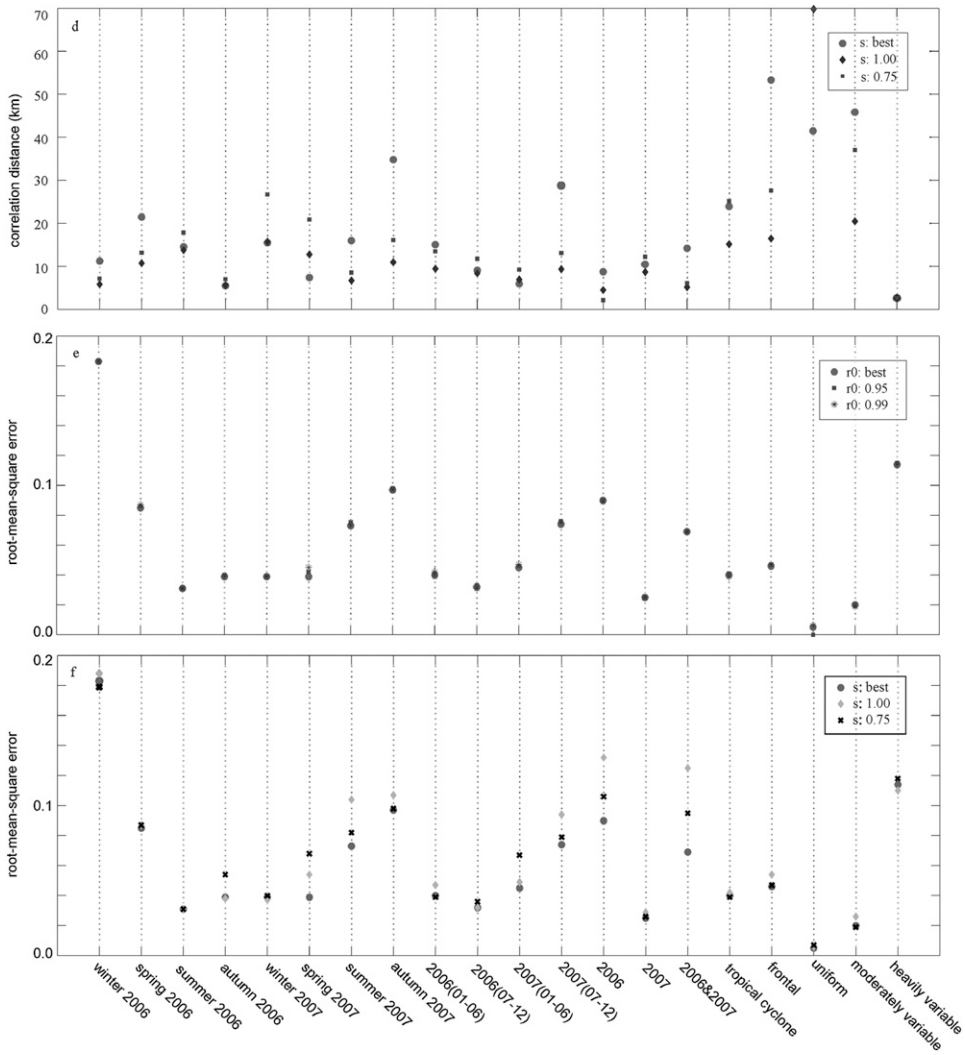

FIG. 12. (*Continued*)

nugget parameter-based values during winter and spring 2007, the first 6 months of 2007, as well as uniform rain (Fig. 12c). The rmse, on the other hand, has almost no difference between its best and predetermined nugget parameter-based values (Fig. 12e).

The correlation distance showed major differences between its best and predetermined shape parameter-based values in a majority of the observations (Fig. 12d). The difference between the best and predetermined shape parameters was correlated to the difference in correlation distances. When the best shape parameter was about 1.0, which was also one of the predetermined shape parameters, there was almost no difference in correlation distances between the two estimates during autumn 2006, winter 2007, and highly variable rainfall. At the same time, a 65% increase in correlation distance was evident between the best (1.73) and predetermined (0.75) shape parameter fittings during spring 2007. The correlation distances were unrealistically high for the predetermined shape parameter for the uniform rainfall.

The rmse for the best fit was less than 0.1 for all observational periods except winter 2006 and highly variable rainfall, with rmse of 0.183 and 0.114, respectively (Figs. 12e,f). It differed noticeably for best and predetermined shape parameters during spring and summer 2007, the year 2007, and a 2-yr period, and was higher than 0.1 for a shape parameter of 1.0 for all these four observational periods (Fig. 12f). It also exceeded 0.1 for 2006 when the shape parameter was set to 0.75.

6. Conclusions

An experimental study was conducted to investigate the variability of rainfall at NASA WFF with six dual

gauge sites located along a nearly straight line. A continuous record of rainfall was available from each gauge site during the 2-yr observational period. The maximum gauge separation distance, 5 km, coincided with the TRMM and GPM precipitation radar beamwidth. The number of gauge sites, the distances, and the configuration of the sites may not be ideal for the precipitation radar footprint, but this pilot study provides important messages regarding rainfall variability in a 5-km^2 area. The rich dataset with over 7100 samples allows studying the rainfall variability for a particular season, a 6-month, and annual periods as well as for different weather systems and different uniformity conditions in the rainfall.

Partial beamfilling has been investigated by examining the percent occurrence of the gauge rainfall with respect to the beam rainfall. Here, the beam rainfall refers to the areal average rainfall. Therefore, if one of the gauges reports rain, the beam will be rainy. For the 2-yr period at 5-min integration, a single gauge reported rainfall 51%–57% of the time, but this range was only 43%–48% during spring 2006. If all the gauges were reporting rainfall, an individual gauge had at most ±13% difference from the areal average rainfall. This suggests that at the spatial scale of 5 km, the variability arising from rain gradients is relatively less important than the variability caused by partially filled footprints.

Temporal sampling from remote sensing instruments has been addressed by recalculating monthly rainfall at different sampling intervals. The sampling at 3- and 12-h intervals resulted in 35% and 73% errors on average in the monthly rainfall estimate. This suggests that a polar-orbiting satellite alone may not be adequate to determine the monthly rainfall. Rather, multisatellite measurements (e.g., TMPA) should be utilized for more accurate monthly rainfall.

A three-parameter stretched exponential model has been fit to the correlations at 15 different gauge separation distances. The nugget parameter was calculated from collocated gauge observations from the G03 site and was an input to the exponential model, while the correlation distance and shape parameters were determined by minimizing the rmse in correlations. All three parameters of the stretched exponential model increased along with decreases in the rmse with longer integration periods. The stretched exponential model was sensitive to the rain–no-rain threshold. The correlations were lower at higher rain–no-rain thresholds, becoming less than 0.2 at 2-mm threshold at 5-km distance.

The parameters of the stretched exponential model differed substantially between the seasons and between the longer observational periods. The nugget parameter was as low as 0.88 during the first 6-month period of 2007 but above 0.95 for most of the seasons and other longer observational periods. The correlation distance ranged from 5 to 35 km between the seasons and it was 14 km for the 2-yr period. The shape parameters ranged from 0.37 and 1.73 for different observational periods but remained less than 1.0 except for three seasons and one of the 6-month periods. During frontal rain, the correlation distance had the highest best fit value, 53 km, than any climatological duration. The correlation distance was relatively high for the tropical cyclone rainfall as well. This was mainly due to the fact that all gauge sites reported rain during the passage of these weather systems most of the time and the spatial variability was relatively less than the partially covered experiment area. The correlation distances had a sharp drop from moderately variable to highly variable cases where it was 3 km—the lowest of all different experimental periods.

The sensitivity of the parameters of the stretched exponential model was tested by selecting two nugget and two shape parameters. The correlation distance was sensitive to the changes in the nugget parameter but considerably more to the shape parameter. Therefore, in the absence of collocated gauges, it is better to assume the nugget parameter from previous studies (such as this one) and apply the best fit to determine the correlation shape and shape parameters.

It should be pointed out that the stretched exponential model tends to determine the correlation at a given distance for 20 different study periods and it should not be used to extrapolate the correlation beyond the maximum gauge separation distance. Another gauge network where the gauge spacing ranges from 5 to 150 km in the southern Delmarva Peninsula is currently operating and it is anticipated that a similar study will be conducted to address the spatial variability of rainfall from microwave sensors on board various polar-orbiting satellites. As noted in the introduction, the IFOV of microwave-sensor-based precipitation estimates is much larger than that of precipitation radars.

Acknowledgments. We thank our senior technician, Paul G. Bashor of Computer Science Corporation, NASA Wallops Flight Facility for his dedicated work on operating the gauge network and reviewing this manuscript. Discussions with Prasun Kundu of the University of Maryland, Baltimore County; S. Joseph Munchak of the University of Maryland, College Park; and Robert Meneghini of NASA Goddard Space Flight Center were very helpful. Thanks to David A. Marks of Science Systems Applications Inc., and Amy J. Houghton of the University of Maryland, Baltimore County for the review. Special thanks to Drs. Emad Habib of the University of Louisiana at Lafayette, Gabriele Villarini of Princeton University, and an anonymous reviewer for

their constructive reviews. This work has been conducted during the second author's visit to the NASA GSFC as a GEST fellow. This work is funded through NASA under Grant NNX07AF45G.

REFERENCES

Bell, T. L., and P. K. Kundu, 1996: A study of the sampling error in satellite rainfall estimates using optimal averaging of data and a stochastic model. *J. Climate,* **9,** 1251–1268.

Ciach, G. J., 2003: Local random errors in tipping-bucket rain gauge measurements. *J. Atmos. Oceanic Technol.,* **20,** 752–759.

——, and W. F. Krajewski, 2006: Analysis and modeling of spatial correlation structure in small-scale rainfall in central Oklahoma. *Adv. Water Resour.,* **29,** 1450–1463.

Datta, S., W. L. Jones, B. Roy, and A. Tokay, 2003: Spatial variability of surface rainfall as observed from TRMM field campaign data. *J. Appl. Meteor.,* **42,** 598–610.

Gebremichael, M., and W. F. Krajewski, 2004: Assessment of the statistical characterization of small-scale rainfall variability from radar: Analysis of TRMM ground validation datasets. *J. Appl. Meteor.,* **43,** 1180–1199.

Habib, E., and W. F. Krajewski, 2002: Uncertainty analysis of the TRMM ground-validation radar-rainfall products: Application to the TEFLUN-B field campaign. *J. Appl. Meteor.,* **41,** 558–572.

——, ——, and G. J. Ciach, 2001: Estimation of rainfall interstation correlation. *J. Hydrometeor.,* **2,** 621–629.

——, B. F. Larson, and J. Graschel, 2009: Validation of NEXRAD multisensory precipitation estimates using an experimental dense rain gauge network in south Louisiana. *J. Hydrol.,* **373,** 463–478.

Hou, A., G. S. Jackson, C. Kummerow, and C. M. Shepherd, 2008: Global Precipitation Measurement. *Precipitation: Advances in Measurement, Estimation, and Prediction,* S. Michaelides, Ed., Springer, 131–169.

Huffman, G. J., and Coauthors, 2007: The TRMM Multisatellite Precipitation Analysis (TMPA): Quasi-global, multiyear, combined-sensor precipitation estimates at fine scales. *J. Hydrometeor.,* **8,** 38–55.

Iguchi, T., T. Kozu, R. Meneghini, J. Awaka, and K. Okamoto, 2000: Rain-profiling algorithm for the TRMM precipitation radar. *J. Appl. Meteor.,* **39,** 2038–2052.

Krajewski, W. F., and J. A. Smith, 2002: Radar hydrology: Rainfall estimation. *Adv. Water Resour.,* **25,** 1387–1394.

——, G. J. Ciach, and E. Habib, 2003: An analysis of small-scale rainfall variability in different climatic regimes. *Hydrol. Sci. J.,* **48,** 151–162.

Kummerow, C., 1998: Beamfilling errors in passive microwave rainfall retrievals. *J. Appl. Meteor.,* **37,** 356–370.

——, W. Barnes, T. Kozu, J. Shiue, and J. Simpson, 1998: The Tropical Rainfall Measuring Mission (TRMM) sensor package. *J. Atmos. Oceanic Technol.,* **15,** 809–817.

Kundu, P. K., and T. L. Bell, 2003: A stochastic model of space-time variability of mesoscale rainfall: Statistics of spatial averaging. *Water Resour. Res.,* **39,** 1328, doi:10.1029/2002WR001802.

Liao, L., and R. Meneghini, 2009: Changes in the TRMM version-5 and version-6 precipitation radar products due to orbital boost. *J. Meteor. Soc. Japan,* **87A,** 93–107.

——, ——, and T. Iguchi, 2001: Comparisons of rain rate and reflectivity factor derived from the TRMM precipitation radar and the WSR-88D over the Melbourne, Florida, site. *J. Atmos. Oceanic Technol.,* **18,** 1959–1974.

Moore, R. J., D. A. Jones, D. R. Cox, and V. S. Isham, 2000: Design of the HYDREX rain gauge network. *Hydrol. Earth Syst. Sci.,* **4,** 521–530.

Nakamura, K., and T. Iguchi, 2007: Dual-wavelength radar algorithm. *Measuring Precipitation from Space,* V. Levizanni, P. Bauer, and F. J. Turk, Eds., Springer, 225–234.

Takahashi, N., H. Hanado, and T. Iguchi, 2006: Estimation of path-integrated attenuation and its non-uniformity from TRMM/PR range profile data. *IEEE Trans. Geosci. Remote Sens.,* **44,** 3276–3283.

Varma, A. K., G. Liu, Y.-J. Noh, 2004: Subpixel-scale variability of rainfall and its application to mitigate the beam-filling problem. *J. Geophys. Res.,* **109,** D18210, doi:10.1029/2004JD004968.

Villarini, G., and W. F. Krajewski, 2008: Empirically-based modeling of spatial sampling uncertainties associated with rainfall measurements by rain gauges. *Adv. Water Resour.,* **31,** 1015–1023.

——, P. V. Mandapaka, W. F. Krajewski, and R. J. Moore, 2008: Rainfall and sampling uncertainties: A rain gauge perspective. *J. Geophys. Res.,* **113,** D11102, doi:10.1029/2007JD009214.

Wang, J., and D. B. Wolff, 2010: Evaluation of TRMM ground-validation radar-rain errors using rain gauge measurements. *J. Appl. Meteor. Climatol.,* **49,** 310–324.

Wolff, D. B., D. A. Marks, E. Amitai, D. S. Silberstein, B. L. Fisher, A. Tokay, J. Wang, and J. L. Pippitt, 2005: Ground validation for the Tropical Rainfall Measuring Mission (TRMM). *J. Atmos. Oceanic Technol.,* **22,** 365–380.